

Artificial Neural Networks for Inverse Problems in Damage Detection using Computational and Experimental Eddy Current

Sekoura Benissad^{1*}, Mokhtar Touati¹, Mohamed Chabaat¹

¹ Built Environmental Research Lab., Dept. of Structures and Materials, Civil Engineering Faculty, University of Sciences and Technology Houari Boumediene, B.P 32 El Alia Bab Ezzouar, 16111 Algiers, Algeria

* Corresponding author, e-mail: sbenissad@usthb.dz

Received: 01 June 2022, Accepted: 08 September 2022, Published online: 19 September 2022

Abstract

A new method for computing fracture mechanics parameters applicable for measuring tests relying on Eddy currents is proposed. This method is based on inverting Eddy current with simultaneous use of Artificial Neural Networks (ANN) for the localization and the shape classification of defects. It allows the reconstruction of cracks and damage in the plate profile of an inspected specimen to assess its material properties. The procedure consists on inverting all the Eddy current probe impedance measurements which are recorded according to the position of the probe, the excitation frequency or both. In the non-destructive evaluation by Eddy currents or in the case of an inverse problem which is difficult to solve, results from a lot of variety of concepts such as physics and complex mathematics are needed. The corresponding solution has a significant impact on the characterization of cracks in materials. On the other side, a simulation by a numerical approach based on the finite element method is employed to detect cracks in materials and eventually, study their propagation. It is shown here that this method has emerged as one of the most efficient techniques for prospecting cracks and enables the study of an increase in size of cracks and its propagation in aluminum material. Besides, it can easily predict future defects in different mechanical parts of a given material and be useful in the treatment of materials than the process of changing parts. It has been proven that it gives good results and high performance for different materials.

Keywords

crack, eddy current, artificial neural network, fem

1 Introduction

In the aircraft industry as well as in the majority of industries, the brutal fracture problem has a great importance. This scientific phenomenon is a very serious problem for a large community of researchers. It leads to the need for a better understanding of the behavior of cracked structures. It is a scientific challenge that represents an important issue from an analytical point of view, numerically as well as experimentally [1]. Non-Destructive Tests (NDT) can make the difference between life and death. Jeffrey T. Fong and testing materials (ASTM) aim to detect defects while preserving the integrity of the product. Thus, the toughness is often measured as a point value and characterized by a parameter such as the Stress Intensity Factor (SIF) or the Energy Release Rate (G) at the crack initiation. The first fracture toughness test standard ASTM E399 was developed to determine the point value of plane strain fracture toughness near to the onset of crack initiation K_{Ic} [2, 3].

NDT by Eddy current testing can be used for a variety of applications such as detection of cracks (discontinuities), measurement of metal thickness, detection of metal thinning due to corrosion and erosion, such as stress-corrosion cracking, fatigue cracks, or inter-granular attack determination of coating thickness and also the measurement of electrical conductivity and magnetic permeability [4]. Eddy current technique (ECT) is an excellent method for detecting surface and near surface defects when a probable defect location and orientation are well known [5]. ECT technique is based on the electromagnetic induction principle for detection the magnetic field due to the Eddy current induced on the test sample. The presence of the defect alters the Eddy currents pattern and causes field's perturbations closely linked to the position and shape of the defect.

An excitation field is carried out by using a coil fed by an alternating current, where the changed impedance coil

can be calculated. This latest considers that a defect has an effect on the induced currents. The modeling of a practical configuration of ECT sensor requires extended analytical or numerical developments because of its complexity. Then, Finite Element Method (FEM) is more general, numerically superior. FEM is mainly used for its versatility modeling of material properties, simulations of boundary conditions as well as modeling arbitrary domain spaces. It also reduces substantially the experimental work [6, 7]. It has also been proven that in a lot of chosen models, the model which satisfies the boundary conditions and takes in consideration applied loads, gives good results.

In order to estimate the material properties of an inspected sample of electrical conductivity profile, the problem of inverse Eddy currents can be described as a task of reconstructing the sample [8]. This is done by inverting Eddy current probe impedance measurements which are recorded as a function of probe position, excitation frequency or both. It is widely recognized as a complex theoretical problem, in a non-destructive evaluation by eddy currents and its solution is likely to have a significant impact on the characterization of conductive materials [9]. Neurons are the highly interconnected processing elements that make up Artificial Neural Networks ANN. These latest can perform arbitrary mappings between sets of input-output pairs. This procedure is realized by adjustment of the weights of interconnections after training through the presentation of examples. Neural network performance has proven robustness when faced incomplete, fuzzy or novel data [10].

In this research work, a new method of calculating fracture mechanics parameters using Eddy current NDTs linked to experimental data is presented. An inverse problem using ANN that simulates the mapping between Eddy current signals and crack profiles is the basis of this method. On the other side, this method is very useful for locating and classifying simultaneously the shape of defects in the spontaneous use of ANN.

2 Eddy current governing equations

FEM computational model is based on the strong coupling of the magnetic field magneto-dynamic equation expressed in terms of magnetic sector potential and the total current density equation composed by the source and eddy current densities. The effectiveness of the proposed model is investigated through the comparison of the impedance with the classical current fed model where massive or multi conductor sensors configurations avoid skin and proximity effects in 2-D and 3-D [11, 12]. These models are numerically

solved using FEM to obtain the Eddy currents distributions in order to calculate the impedance variation at each sensor position as well as to show the advantage and effectiveness of the Model (A-J). ECT phenomenon can be treated as a quasi-static electromagnetic field problem expressed by the governing field equations in terms of electrical scalar and magnetic vector potentials. These equations can be solved by 3-D FEM. Application of the Coulomb gauge allows simultaneous solution of the coupled magnetic vector potential and electric scalar potential equation in the inductor Ω_i and the conducting region Ω_c , the non-conducting region representing the air Ω_a with a current density source. These equations can be written as,

$$\nabla \times (v \nabla \times A) - \nabla (v_p \nabla \cdot A) \begin{cases} 0 & \text{in } \Omega_a \\ J_s & \text{in } \Omega_i \\ -J\omega\sigma(A + \nabla \cdot v) & \text{in } \Omega_c \end{cases}, \quad (1)$$

$$\nabla \cdot v (J\omega A + \nabla \cdot v) = 0, \quad (2)$$

where J_s the current density source, v_p is the penalty term, v corresponds to the magnetic reluctivity, ∇ is the electrical potential, σ is the electric conductivity and ω is the angular frequency. The integral $A \cdot V$ is obtained when applying Galerkin's methods and the weighted residuals for Eqs. (1) and (2), using vector N_i and scalar α_i weighted functions. Such a formulation leads to the following integral form [1, 12].

$$\int_{\Omega} v (\nabla \times N_i) \cdot (\nabla \times A) + v_p (\nabla \times N_i) (\nabla \times A) d\Omega = \int_{\Omega} J\omega\sigma (N_i A + \alpha_i V) d\Omega \quad (3)$$

$$\oint_{\Gamma} N_i v (\nabla \times A) d\Gamma = \oint_{\Omega} N_i J_s d\Omega \quad (4)$$

$$\int_{\Omega} J\omega\sigma [\nabla (N_i A + \alpha_i V)] d\Omega = 0 \quad (5)$$

3 Sensor impedance calculation

The detection of change of the resulting magnetic fields is based on two basic methods: the NDT differential mode represented by two separate coils linked magnetically and supplied by the same current and the NDE absolute mode which makes use of only one coil. The impedance variation is obtained from comparison with the reference impedance. The impedance variation ΔZ is a complex number. The imaginary part is computed with the magnetic energy (W_M) in the whole meshed domain and the real part is computed with the Joule Losses in the conductive media and

the imaginary part is computed with the magnetic energy in the whole meshed domain. The coil impedance with an excited current I at a frequency F is obtained by the following expression [8].

$$\begin{cases} R_e(Z) = \frac{JL}{I^2} \\ R_e(\Delta Z) = \int_{\Omega_c} \frac{1}{\sigma} (|J_f^2| - |J|^2) d\Omega \end{cases}, \quad (6)$$

$$\begin{cases} Im(Z) = \frac{\omega W_M}{I^2} \\ Im(\Delta Z) = \omega \int_{\Omega_c} \frac{1}{\mu} (|B_f^2| - |B|^2) \end{cases}, \quad (7)$$

$$\begin{cases} Z = R + jX \\ Z = \frac{1}{I^2} \left(\int_{\Omega} \frac{J^2}{\sigma} d\Omega + j2\Pi F \int_{\Omega} (B.H) d\Omega \right) \end{cases}, \quad (8)$$

where, B and H are the induced magnetic induction, and the magnetic field, respectively

4 Application

In this section, we test a magnetic plate without any crack characterized by permeability equal to the unit, a high conductivity 10^6 (Sm^{-1}), excited by a sinusoidal current of density of current $I = 2.67 \cdot 10^6$ (A/m) and a frequency of 10 kHz. EC testing problem deals with a Pancake coil placed above a flat plate, as shown in Fig. 1, with a rectangular crack. The coil is set along the crack length direction, moving in the xy plane, parallel to the x-axis. Besides, planar visualization in 3-D mesh is presented in Fig. 1 [12].

5 Results interpretation

The result of simulation obtained in the case of a non-magnetic plate without defects are illustrated by a set of figures as follows: Figs. 2, 3 and 4 present the distribution of the representation of the potential magnetic Vector A_x , A_y ,

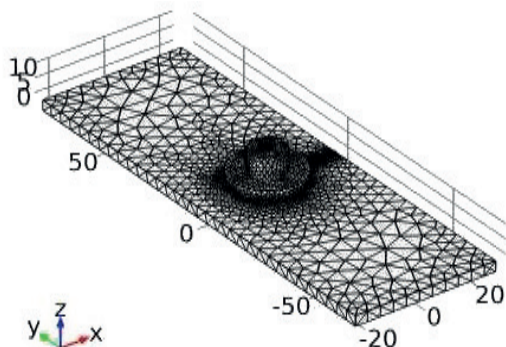


Fig. 1 Planner visualization of the 3D mesh around the coil

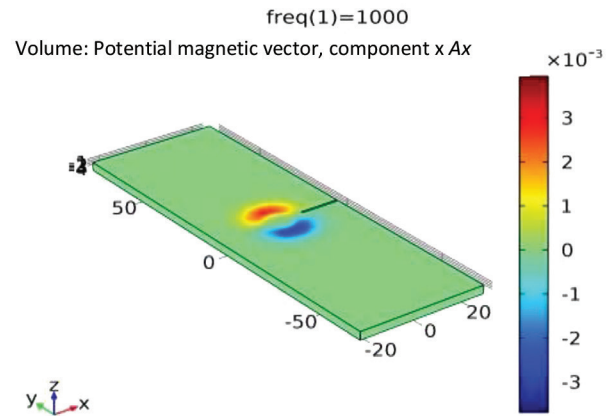


Fig. 2 Representation of the potential A_x

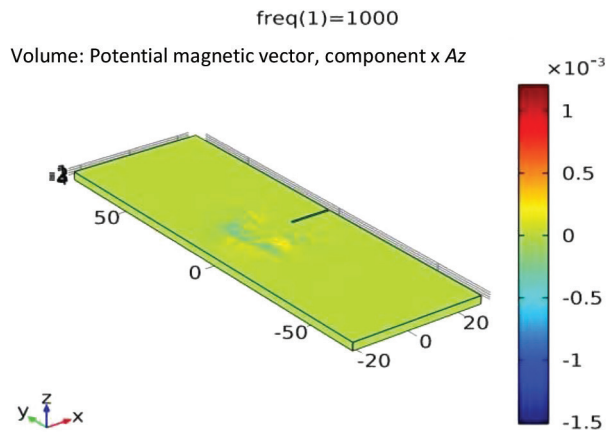


Fig. 3 Representation of the potential A_z

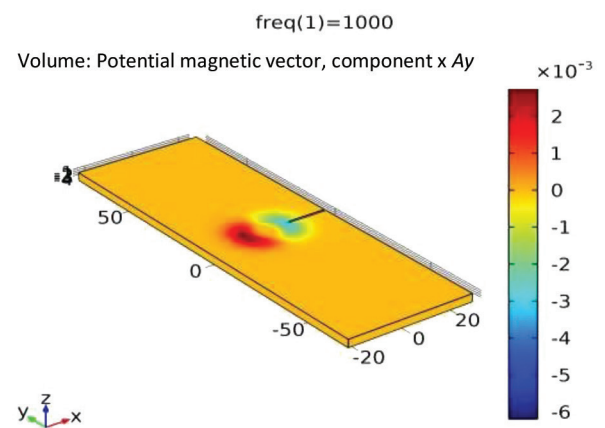


Fig. 4 Representation of the potential A_y

and A_z , respectively. They expose a great power of concentration of the potential to the level of the conductor and cracks and show weaknesses in values from where high use of the frequency. Fig. 5 represents the distribution of the currents induced on the surface of target. It is noticed that their values are high because the conductivity of the non-magnetic target is large ($j = \sigma \cdot 2\pi \cdot f \cdot A$) but are relatively weak compared to the primary currents. Fig. 6 indicates

the distribution of the magnetic field. That explains the strong concentration of the vectors of magnetic induction on the level of the cracks without the possibility to penetrate inside the plate due to the characteristics of the material and the effect of the frequency. In Figs. 7 and 8, one can notice that when the width decreases, the value of impedance Z decreases at the same rate. The width of the defect has a great influence on the variation of impedance. Besides, the variation depth of the defect has a light influence on Z . It is also noticed that the difference of impedance Z has dependence with the width of the defect; indeed, the width of defect increases Z automatically and consequently; it can be evaluated. On the opposite, Z decreases when the width decreases, leading us to conclude that the depth of defect does influence the impedance. The variation depth of the defect has a feathery influence on Z .

6 Experimental test set up

The experimental test is set up as shown in Fig. 9. The diameter of the prototype differential ECT sensors is 100 mm and the lift-off in test is 0.5 mm. The specimen used in test is an aluminum plate of 3 mm thickness. There are four slots

having a deep length of 2 mm, 1.5 mm, 1.0 mm and 1.0 mm, respectively. A 1.5 mm wide slid is made in the specimen to simulate surface cracks. As we know, the higher the excitation frequency is, the smaller is the standard penetration depth. ECT sensor excited by high frequency can be sensitive to surface cracks. For an aluminum material, the room conductivity is taken to be 10^7 Sm^{-1} and the magnetic permeability μ is 10^{-6} H/m , excited by a sinusoidal current of density of current $J = 2.67 \cdot 10^6 \text{ A/m}$ and a frequency of 10 kHz. In this part, an approach for studying the measured impedance of the measured impedance in the inductive sensor is proposed, for the non-destructive testing by Eddy currents in an absolute mode. The equivalent circuit of eddy current testing is shown in Fig. 9 [13].

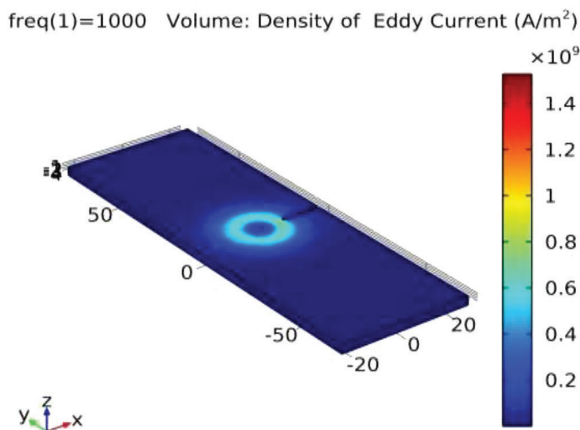


Fig. 5 Density of the induced current I

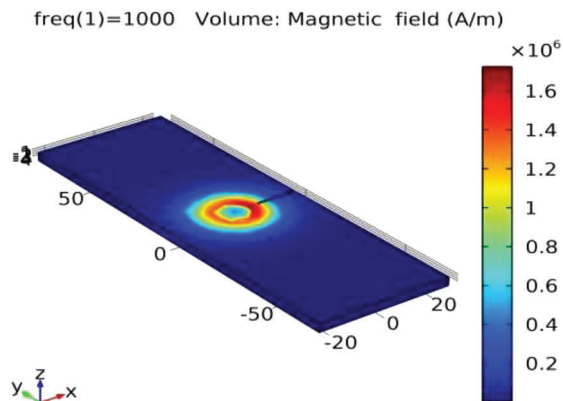


Fig. 6 Vector of magnetic induction B

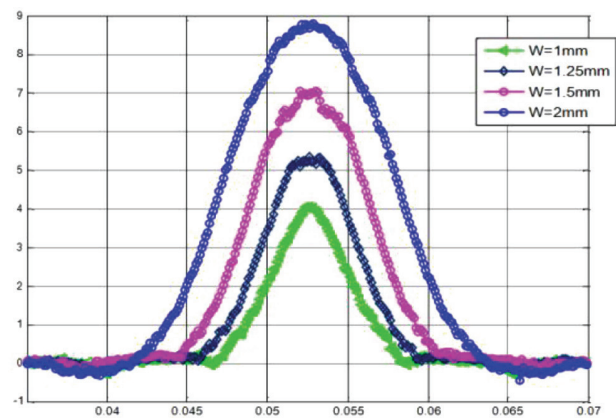


Fig. 7 Impedance ΔZ vs the different cracks width

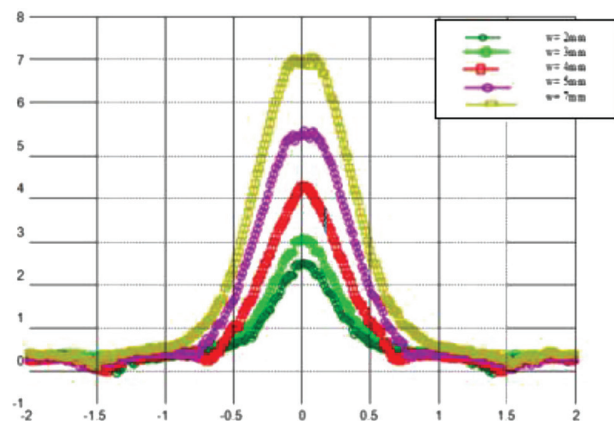


Fig. 8 Impedance Z vs different cracks depth

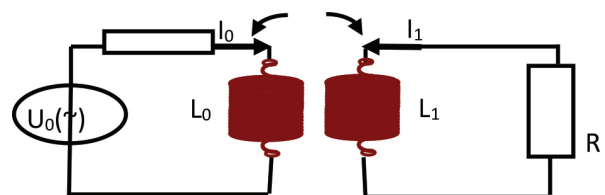


Fig. 9 Equivalent circuit of Eddy current testing

Circuit 1:

$$U_0 = R_0.i_0 + L_0.\frac{di_0}{dt} + M.\frac{di_1}{dt} \quad (9)$$

Circuit 2:

$$R_1.i_1 + L_1.\frac{di_1}{dt} + M.\frac{di_0}{dt} = 0, \quad (10)$$

where f is the excitation frequency of coil; R_0 , and L_0 are the resistance and inductance of coil, respectively. R_e and L_e are the resistance and inductance of the induced eddy current loop. M is the mutual inductance between the two loops.

The circuit solution is given by the equivalent impedance Z in Eq. (11). It is composed of a resistance and an inductive reactance. We notice that Eqs. (12) and (13) given bellows indicate that the equivalent resistance R increases while the equivalent inductance L decreases due to induced Eddy currents.

$$\underline{Z} = R + jL\omega \quad (11)$$

The resistance is given as follows.

$$R = \left(R_0 + \frac{M^2.\omega^2.R_1}{R_1^2 + L_1^2\omega^2} \right), \quad (12)$$

and the primary inductance is by;

$$L = \left(L_0 - \frac{M^2.\omega^2.L_1}{R_1^2 + L_1^2\omega^2} \right). \quad (13)$$

When the ECT sensor tests a surface crack, the existence of defect affects the coupling between excitation coil circuit and Eddy current loops. The coupling can be interpreted as mutual inductance M that is dependent on the crack characters like the position, the size, the depth, the extension direction and the shape [9].

Experimental results obtained from the different tests are plot in the following Figs. 10, 11, and 12. Numerical plots are also drawn in the same figures. As one can notice, values of the impedance Z are in good agreements between both experimental testing and numerical method. It is proven that the numerical model fit well with expected results found from experimental test.

7 Artificial neural networks

Although this is an oversimplified model of the biological brain, the organization and the information processing strategies of an ANN are based on the features of their biological counterparts. The neurons combine the input impulses in several ways, operating in parallel with other

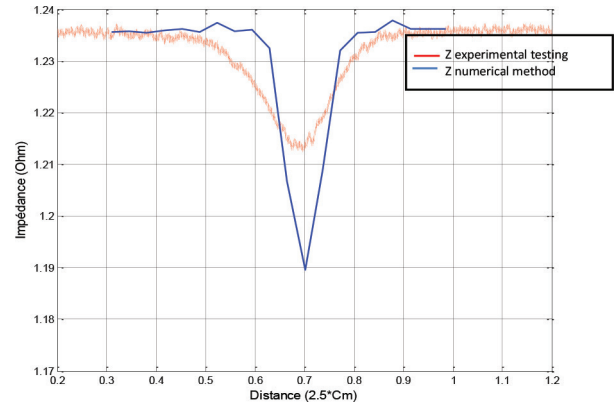


Fig. 10 Impedance Z by experimental testing and numerical method

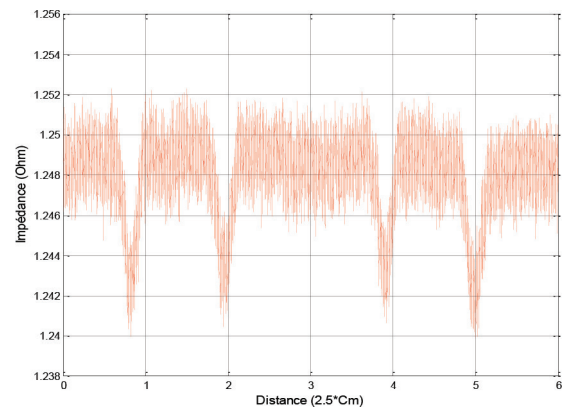


Fig. 11 Impedance Z by experimental testing and numerical method
 $f = 20 \text{ KHz}$

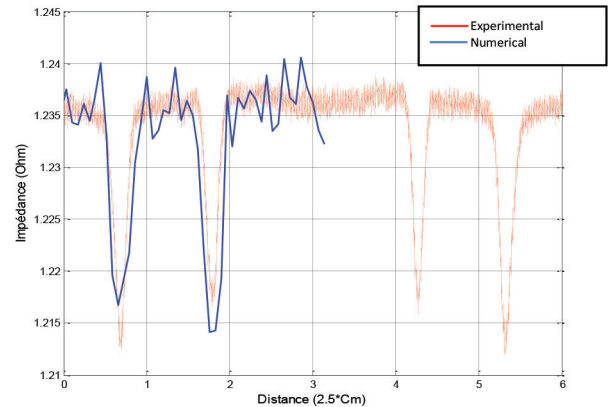


Fig. 12 Impedance Z by experimental testing and numerical method

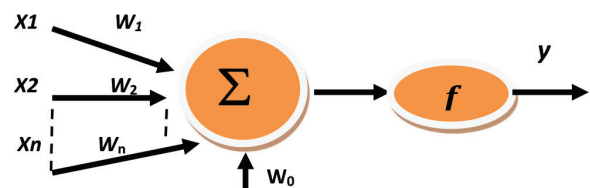


Fig. 13 Skeleton form of Artificial Neural Networks

neurons to perform a variety of functions. In artificial neural nets, each simple node performs a weighted sum of the inputs and computes a nonlinear function of the results.

In the learning process, the actual output of the artificial neuron network is compared with the desired output. Changes are made by modifying the connection weights of artificial neural network to produce a closer match to a neuron that may make a nonlinear function of its inputs. But one neuron is not sufficient in most applications and the association of several neurons can be more preferable. The composition of non-linear functions performed by each neuron is permitted by several neurons associated to the network, which is particularly needed for the modeling systems whose behavior is not simple. The feed forward neural networks (also called feed forward) are represented by a set of connected neurons to each other. Neuron information flows from the inlet to the outlet without return rearward. There are several types of feed forward networks, but in practice, those that are most used are the type MLP (Multilayer Perceptron) [12].

Let's call input parameters, output layers all output neurons. Intermediate layers having no contact with the outside world are called hidden layers. For a given layer, neurons have the same activation function. The output of the ANN is obtained directly after application of the input signal with the propagation times of information very close.

The first formal neuron performs weighted sum inputs ($x_1 \dots x_n$) by the weight ($w_1 \dots w_n$) connections which are added through w_0 . Then, this value is subjected to an activation function f whose result is the Y output of the neuron as shown in Fig. 13.

From the above description, the output of the neuron can be written as

$$y_i = f\left(\sum_1^n w_i X_i + w_0\right). \quad (14)$$

The behavior of a neuron is fully described by both the value of its connections and its function activation. This latest is known as a sigmoid function.

$$f(x) = \frac{1}{1 + e^x}, \quad (15)$$

where w_{ij} is the weight coefficient, x_j is the input signals, and y_j is the output at the neuron i of the output layer.

In this research work, ANN procedure along with FEM analysis and experimental testing is used to solve inverse problems that are met in the detection of cracks. This approach can be able to identify unknown metallic objects as well as internal and external cracks. Simultaneous use of ANN can be very useful for locating and classifying defect shapes. The methodology used in this work consists in feigning signals of a response by the detector

on the influence of physical variations and geometrical parameters of the metallic objects that are buried by FEM and Experimental Testing. Obtained results (profiles) are used to generate a base (basis) of learning (apprenticeship) of a model of networks of neurons multi-coats (multilayer) or MLP (Multilayer-Perceptron) [12].

8 Model validations

Application of NN to the inversion method of the probe coil impedance is tested to identify and evaluated the form of cracks. NN input consists in the probe impedance while its output provides evaluated cracks with different shapes (Fig. 14). An important problem in the NN inversion process is the selection of the network structure and the adjustment of internal parameters. The determination of the optimal NN structure and the test are realized by the improbability method. Data sets are created by data thanks to the problem of the electromagnetic interaction between the probe and plate by using FEM. Every set contains the input-output data belonging to the evaluation range. The training set allows to train the NN, meaning, the adjust of internal parameters. Neural network is performed by minimizing the mean square error (MSE) which is used as a cost function and measured between the output of the network and the desired solution when corresponding inputs are presented to the NN. The mean square error value is computed by [12].

$$MSE(w) = \frac{1}{N} \sum_{k=1}^N D_k - S(E_k, w)^2, \quad (16)$$

where, E_k is the input vector, D_k is the desired output vector, w corresponds to the constituted column vector of the set of the weights and bias of the network, S is a realized function by NN, and N is the number of samples in the training set [7].

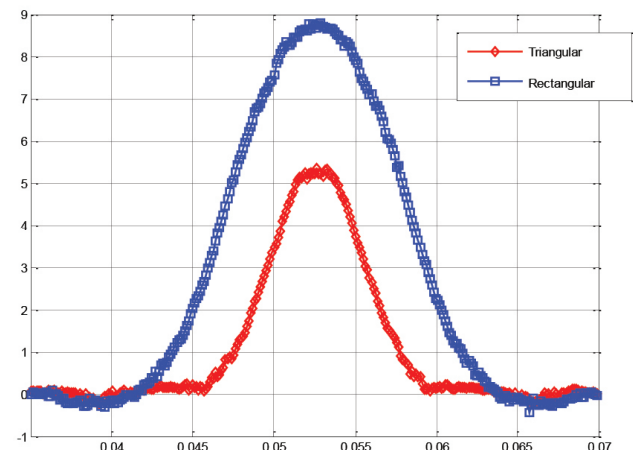


Fig. 14 Impedance Z vs. different crack's shapes

In this study, results of the various cases of simulation have been obtained. From these results, one can conclude that: The calculation of the impedance in only one point is not enough to confirm the presence or the absence of a defect in materials. This confirmation leads us to the calculation of the impedance along the Plate. The detection of an external defect requires the energy of the sensor by high frequencies. The position of defect (internal, in the middle, external) has a large effect on the impedance. The use of this sensor type in industrial application is frequent because of its precision. On the other side, this type of sensor lies in the fact that it is unable to detect a defect.

The accuracy and performance of the derived correlations was evaluated on the basis of the following statistical error tests which are coefficient of determination R^2 , root mean square error (RMSE) and its normalized value (nMBE), relative root mean square error (rRMSE), mean absolute error (MAE) and its normalized value (nMAE). These error indices are defined as [12],

$$RMSE = \sqrt{\frac{1}{n} \sum_{i=1}^n (y_i - x_i)^2}, \quad (17)$$

$$rRMSE = \frac{\sqrt{\frac{1}{n} \sum_{i=1}^n (y_i - x_i)^2}}{\frac{1}{N} \sum_{i=1}^n X_i} \times 100. \quad (18)$$

The ranges of rRMSE define the model performance as:

Excellent if: $rRMSE < 10\%$

Fair if: $12\% < rRMSE < 30\%$

Good if: $10\% < rRMSE < 20\%$

Poor if $rRMSE > 30\%$

$$MAE = \frac{1}{N} \sum_{i=1}^n |y_i - x_i| \quad (19)$$

$$R^2 = \frac{\sum_{i=1}^n (y_i - x_i)^2}{\sum_{i=1}^n (y_i - \bar{y}_i)^2} \quad (20)$$

Here, y_i and x_i are the estimated and the measured value \bar{y}_i is the average of estimated value and N corresponds to data number.

9 Inversion procedure

The length and width are estimated by a type of neural network (MLP) is employed as in Fig. 15 representing the steps of inversion. Evaluating the depth or length separately does not lead to a complete characterization of the geometry of a crack. From where an evaluation of the two

sizes (depth and length) will be carried out at the same time by exploiting the previous architecture, but in this case the database must contain two input vectors and two output vectors to estimate. Fig. 15 shows a block diagram of a network (MLP) with two inputs and two outputs for the fault characterization. The learning algorithm is repeated several times so that each iteration biases are reset and therefore, the results can be different. On the other hand, Fig. 16 shows the cost function (MSE), and we remark that it converges to the optimum imposed 5.10^{-7} after 122 iterations. It represents also the linear regression between the desired output and the output of the network; we notice that there is a very good correlation between the real values of the crack and those estimated by the neural network. Finally, we obtain the global geometric shape of the defect; with the driving of the network (MLP) and the cost function (MSE), we notice that it converges to the optimum imposed (the mean square error (MSE) reached the optimum of 10^{-7}).

Results from the FEM for each figure have been inversed just for comparisons purposes with the ANN optimization and the true profile of the shape crack. These comparisons are shown in Figs. 17, 18 and 19 and give good maps representing the NN in very short time.

10 Conclusions

A Finite element discretization of 3-D for solving problem in Eddy current testing is presented in this paper. The main idea is the introduction of categorization for the shape

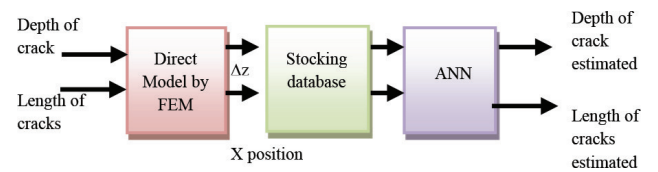


Fig. 15 Inverse problem ANN

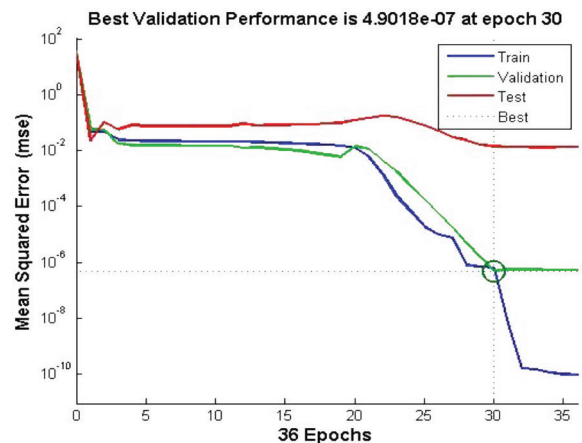


Fig. 16 Cost's function (MSE) vs. number of epochs

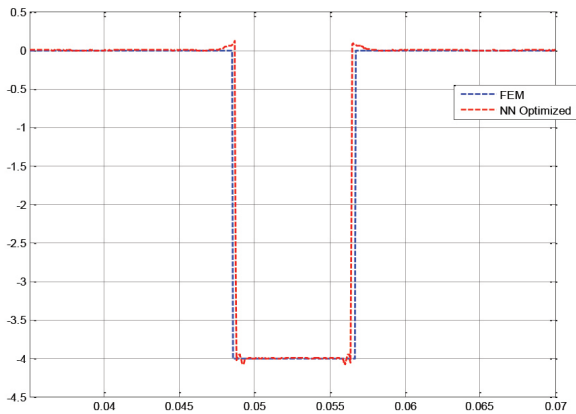


Fig. 17 Comparison results from the ANN optimized and FEM profile (rectangular crack)

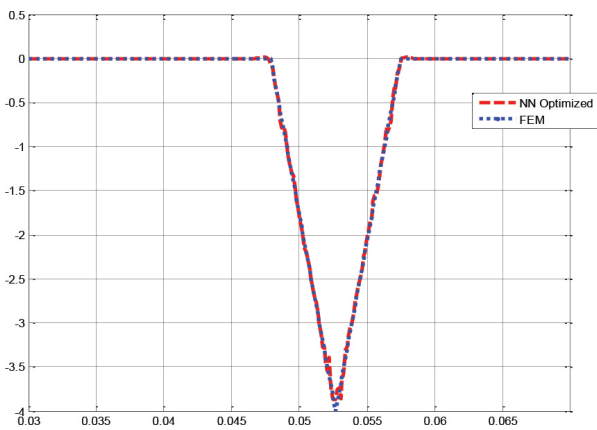


Fig. 18 Comparison results from the ANN optimized and FEM profile (triangular crack)

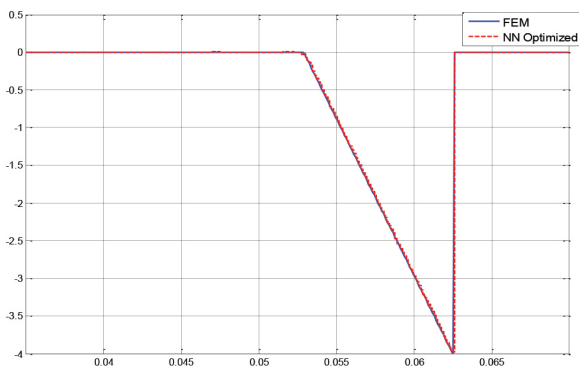


Fig. 19 Comparison results from the ANN optimized and FEM profile (triangular crack)

reconstruction using the NDT by 3D-EC. Results are presented for a simple Eddy current problem using the finite element method as an experimental support. Eddy current testing responses which estimate the forms of crack are obtained by the inverse model in a very short time. This model has given reasonable results. On the other side, it is

very important to make sure that the application in 3-D Eddy current for various cases of simulations can be a good substitute and also very helpful in the NDT operators' work. Besides, the application consists to simultaneously estimate the two parameters of the crack: depth and length.

In this research paper, a neural network for application in the field of (NDT-EC) is developed. This is just to restore the geometrical shape of a defect type which is considered as a lack in the material. This can be done through the estimation of its dimensions (length and depth). Thus, a reverse problem is solved by a MLP neural network whose activation function is the function (logsig) that has been operating in this part. So as the sensor used in this work is of a differential type, then we have chosen two real and imaginary parts of each impedance constituting the sign of defect, in order to achieve a match between the data of the direct problem and those got by the neuron network in an acceptable time. Obtained results have shown similarities between those of a direct model with an ANN model, which proves that we can reach more important goals such as the characterization of defects, something that was not accessible through the direct model. It is very important to make sure that application of artificial intelligence will be a good substitute or help of the NDT operators' work.

Besides, we noticed that the obtained results are identified by flocculation of impedance of the magnetic current value. These values agreed with the previous results. They can allow us to determine the mechanical properties of the material as well as the fracture parameters such as expansion and crack propagation. In this study, this new approach can predict easily future damage of mechanical parts. Except that this technology can direct us to the treatment of materials instead of changing parts of them. It gives accurate results and high performance for parts of materials Possible prediction of cracks propagation through the determination of fracture parameters such as the stress intensity factor SIF and J-integral using Eddy current. Similar results are obtained using theoretical methods for both parameters SIF and J-integral.

The use of this method in industrial application is frequent because of its precision (minimal error) and its low costs.

Acknowledgment

The Authors thank the Built Environment Research Laboratory (USTHB) and the General Direction of Scientific Research and Development of Technology (MESRS, Algeria) for their support of this work.

References

- [1] Harzallah, S., Chabaat, M., Chabane, M. "Numerical study of eddy current by Finite Element Method for cracks detection in structures", *Journal of Fracture and Structural Integrity*, 39, pp. 282–290, 2017.
<https://doi.org/10.3221/IGF-ESIS.39.26>
- [2] ASTM "ASTM E399-17 Standard Test Method for Linear-Elastic Plane Strain Fracture Toughness of Metallic Materials", ASTM International, West Conshohocken, PA, USA, 2017.
<https://doi.org/10.1520/E0399-17>
- [3] Knitter-Piątkowska, A., Guminiak, M., Hloupis, G. "Crack identification in plates using I-Dorete wavelet transforms", *Journal of Theoretical and Applied Mechanics*, 55(2), pp. 481–496, 2017.
<https://doi.org/10.15632/jtam-pl.55.2.481>
- [4] Guminiak, M., Knitter-Pitkowska, A. "Selected problems of damage detection in internally supported plates using one-dimensional discrete wavelet transform", *Journal of Theoretical and Applied Mechanics*, 56(3), pp. 631–644, 2018.
<https://doi.org/10.15632/jtam-pl.56.3.631>
- [5] Notghi, B., Brigham, J. C. "Computational approach for robust nondestructive test design maximizing characterization capabilities for solids and structures subject to uncertainty", *International Journal for Numerical Methods in Engineering*, 104(4), pp. 297–311, 2015.
<https://doi.org/10.1002/nme.4945>
- [6] Jomdecha, C., Cai, W., Xie, S., Chen, Z., Li, P. "A numerical study on Eddy current signal characteristics of imitative stress corrosion cracks", *International Journal of Applied Electromagnetic and Mechanics*, 55, pp. 257–269, 2017.
<https://doi.org/10.3233/JAE-170066>
- [7] Wang, J., Tao, Y., Tian, T., Ren, R. "Simulation research on eddy-current loss of cable trench structure of metal top pipe", *International Journal of Applied Electromagnetics and Mechanics*, 56(3), pp. 499–510, 2018.
<https://doi.org/10.3233/JAE-170130>
- [8] Jesenik, M., Beković, M., Hamler, A., Trlep, M. "Searching for hidden cracks and estimations of their depths by using the database", *NDT&E International*, 86, pp. 44–52, 2017.
<https://doi.org/10.1016/j.ndteint.2016.11.007>
- [9] Harzallah, S., Chabaat, M. "3D FEM computation and experimental study of eddy currents for characterization of surface cracks", *International Journal of Structural Integrity*, 8(5), pp. 603–610, 2017.
<https://doi.org/10.1108/IJSI-02-2017-0013>
- [10] Helifa, B., Féliachi, M., Leftaier, I. K., Boubenider, F., Zaoui, A., Lagraa, N. "Characterization of Surface Cracks Using Eddy Current NDT Simulation by 3D-FEM and Inversion by Neural Network", *The Applied Computational Electromagnetics Society Journal (ACES)*, 31(02), pp. 187–194, 2016.
- [11] Babbar, V. K., Underhill, P. R., Stott, C., Krause, T. W. "Finite element modeling of second layer crack detection in aircraft bolt holes with ferrous fasteners present", *NDT & E International*, 65, pp. 64–71, 2014.
<https://doi.org/10.1016/j.ndteint.2014.03.005>
- [12] Rosado, L. S., Santos, T. G., Ramos, P. M., Vilaça, P., Piedade, M. "Differential planar Eddy currents probe: Fundamental modeling and experimental evaluation", *NDT & E International*, 51, pp. 85–93, 2012.
<https://doi.org/10.1016/j.ndteint.2012.06.010>